Proceedings of the American Control Conference
Chicago, Illinois • June 2000

A Model for Friction in Atomic Force Microscopy

S. Salapaka and M. Dahleh
{salpax, dahleh}@engineering.ucsb.edu
Department of Mechanical & Environmental Engineering, UC Santa Barbara, CA 93106.

Abstract

A mass-spring-damper model has been presented to describe the cantilever-sample dynamics in Atomic Force Microscope (AFM). Friction has been incorporated in this model by using Johnson-Kendall-Roberts (JKR) theory for elastic contacts. It has been validated by exhibiting some characteristic features (such as stick-slip behavior) observed in experiments with AFMs. A control law has been designed so that the piezoelectric tube in an AFM moves in a desired manner inspite of the friction. Simulation results have been presented to illustrate the model and performance of the controllers.

Key words : mass-spring-damper model, JKR theory, AFMs, friction, control, tracking, stick-slip, differential inclusions.

Introduction

In this paper, we study tip sample interactions and develop a model for friction in an Atomic Force Microscope (AFM). The operational idea of this tool is to detect the displacements of a microcantilever tip as the sample surface moves under it. A schematic of an AFM is given in Figure 1. It consists of a microcantilever, a sample positioner (the piezo tube), a detection system (the optical head) and a control system. The sample is mounted on a piezoelectric tube scanner. It has the ability of fine displacements in the vertical and the lateral directions. The features on the sample cause the cantilever to deflect in a vertical direction as the sample moves under its tip. A laser beam is focused on the back of the cantilever and the reflected beam is collected by a photodetector. Its output signal is used as the feedback signal to control the vertical position of the piezo tube scanner and the sample, such that the cantilever deflection (hence the normal force at the tip sample interface) will remain constant as the sample is scanned.

The forces and dimensions involved in this setting are very small so that new models are being developed to account for various phenomena that are neglected in large scales [8]. After the invention of the AFM [3, 2, 6], there has been an immense boost to the study of phenomena such as adhesion, friction and wear at the molecular and atomic level. Many experiments have been done to study the effects of various factors, such as geometry, material properties and relative velocities of surfaces sliding over each other. In [10, 17], a systematic experimental investigation of the effects of load, tip geometry, lattice orientation, scanning speed and humidity on the frictional force has been presented. The effect of adhesive forces on friction has been considered in [5]. In [1, 4, 16, 14], models describing the contact and intermittent contact modes of AFM have been presented. In this paper, we develop a model to describe the motions of the cantilever and the sample including the frictional forces and also design control laws so that the scanner moves in a desired manner inspite of these forces.

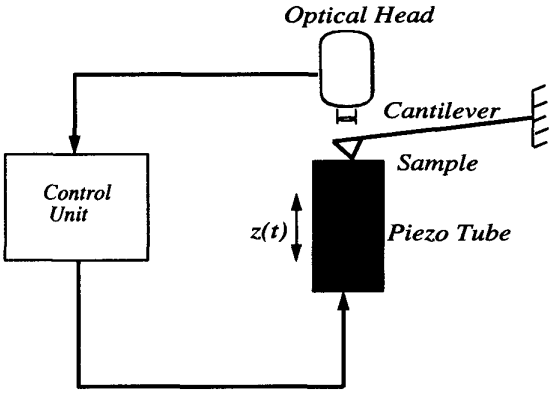

Figure 1: A schematic of an AFM.

1 Johnson-Kendall-Roberts Theory [12]

Johnson-Kendall-Roberts (JKR) theory which we use to model friction. The JKR theory is a continuum contact mechanical model that considers the effect of surface energy on the properties of an elastic contact. The JKR theory allows the determination of several mechanical properties of contact including pressure distribution, indentation depth, contact area etc (see [12, 5]). The radius of contact as a function of the applied load L is given by

$$a = \left(\frac{R_e}{K}[L + 6\pi R_e\gamma + \sqrt{12\pi R_e\gamma L + (6\pi R_e\gamma)^2}]\right)^{\frac{1}{3}},$$

0-7803-5519-9/00 $10.00 © 2000 AACC

where $R_e = RR_s/(R+R_s)$ is the effective radius, R is the tip radius, R_s is the sample radius and γ is the *Dupre energy of adhesion*, which corresponds to work required per unit area to separate the surfaces from contact to infinity. K is the reduced elastic modulus of the two materials given by $K = \frac{4}{3}\left[\frac{1-\nu_1^2}{E_1} + \frac{1-\nu_2^2}{E_2}\right]$, where E_1 and E_2 are the Young's moduli, and, ν_1 and ν_2 are the Poisson ratios of the tip and the sample respectively. Therefore, the contact area is given by

$$A_c = \pi\left(\frac{R_e}{K}\left(L + 6\pi R_e\gamma + \sqrt{12\pi R_e\gamma L + (6\pi R_e\gamma)^2}\right)\right)^{\frac{2}{3}}.$$

The theory predicts that a finite negative load is required to separate the surfaces. This value is referred to as *pull-off force* or *critical load*, given by $L_s = -3\pi R_e\gamma$. The contact area does not diminish to zero (see Figure 2) at this load but has some finite value given by $A_{c_s} = \pi\left(\frac{3\pi\gamma R_e^2}{K}\right)^{\frac{2}{3}}$.

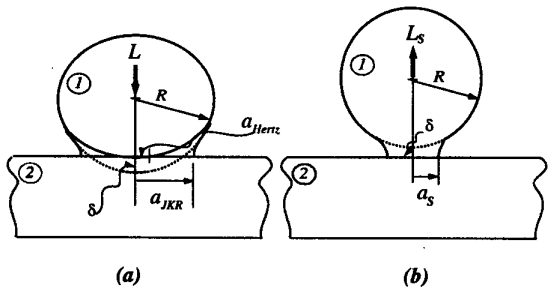

Figure 2: Sphere (of radius R) in contact with a flat (radius = ∞) surface. a_{JKR} and a_{Hertz} are the contact radii predicted by the JKR and *Hertz* theory respectively. δ is the indentation depth and L_s is the critical pull-off load. (a) Here the applied force is pushing one body towards the other. (b) Here the applied force is pulling away the body (1) from the body (2).

Many experiments have shown that the frictional force is proportional to the area of contact [9] and is given by $F_f = \tau A_c$, where τ is the shear strength. The friction at the pull-off load is given by

$$F_{f_s} = \tau A_{c_s} = \pi\tau\left(\frac{3\pi\gamma R_e^2}{K}\right)^{\frac{2}{3}} = \pi\tau\left(\frac{R_e}{K}|L_s|\right)^{\frac{2}{3}}.$$

The expression for friction can be simplified as $\hat{F}_f := \frac{F_f}{F_{f_s}} = \left(1+\sqrt{1+\hat{L}}\right)^{\frac{4}{3}}$, where $\hat{L} := \frac{L}{|L_s|}$. This theory also gives the indentation depth, that is, the height by which the centre of the tip comes down due to flattening of the sphere, $\delta = \frac{a^2}{R_e}\left[1 - \frac{2}{3}\left(\frac{a_o}{a}\right)^{\frac{3}{2}}\right]$, where, $a_o = (12\pi R_e\gamma/K)^{1/3}$, is the radius of contact at no load.

2 Mass-Spring-Damper Model of AFM with Friction

In this section, we study a simple model for cantilever tip-sample interaction with friction in Atomic Force Microscopes. A visualization of the model is given in Figure 3-(I). We model the cantilever as a mass-spring system with mass m_c and natural frequency ω_c. The piezo (along with the sample) is modeled as a mass-spring-damper system with springs and dampers attached to the mass in each direction of motion of the piezo (see Figure 3-(I)). The corresponding mass is m_p, the damping coefficients are ξ_x, ξ_y and ξ_z and the natural frequencies are ω_x, ω_y and ω_z in respective directions. We assume that these springs do not bend, and transmit forces only in one direction. We also assume that the cantilever is in constant contact with the sample (which is ensured by applying a relatively large constant force W on the cantilever), and that the contact areas are formed instantaneously.

Now, we present the reference coordinate-axes in which the equations describing the model dynamics evolve. We call any plane parallel to the axis of the stationary piezo (the spring in the Figure 3-(II)) as the vertical plane and the plane orthogonal to it as horizontal plane. We fix the horizontal plane passing through the equilibrium position of the spring (see plane A in Figure 3-(II)). Note that, in this model we do not consider a point mass for the model of the piezo-sample, but also include the sample surface profile. We fix the origin at the point where the spring (its axis) touches the mass, and the $z = 0$ plane coincides with the bottom plane of the piezo mass (in the model) when no forcing is applied on it. This fixes an orthogonal inertial coordinate system. We also attach another coordinate system which moves along with the piezo sample mass. The origin in this system is taken as the point of contact between the spring and the mass. The coordinates of this origin with respect to the inertial frame will be called the coordinates of the piezo-sample mass. This coordinate system is used only to specify the profile of the sample surface, $h(x,y)$, which is thus made independent of the inertial frame. We attach another inertial frame which is the same as the frame mentioned earlier, but displaced vertically by a distance a with its origin at the equilibrium point of the cantilever (the center of the tip) under no forcing. The forcing functions on the sample (via electrodes on the piezoelectric tube) are given by $m_p u_x(t)$, $m_p u_y(t)$ and $m_p u_z(t)$ in respective directions. The dynamics of the piezo-sample is described by

$$\begin{aligned} m_p\ddot{x} + 2m_p\xi_x\omega_x\dot{x} + m_p\omega_x^2 x &= m_p u_x(t) - F_{r_x}, \quad (1)\\ m_p\ddot{y} + 2m_p\xi_y\omega_y\dot{y} + m_p\omega_y^2 y &= m_p u_y(t) - F_{r_y},\\ m_p\ddot{z} + 2m_p\xi_z\omega_z\dot{z} + m_p\omega_z^2 z &= m_p u_z(t) - N, \end{aligned}$$

where, x, y and z are the coordinates of the piezo-

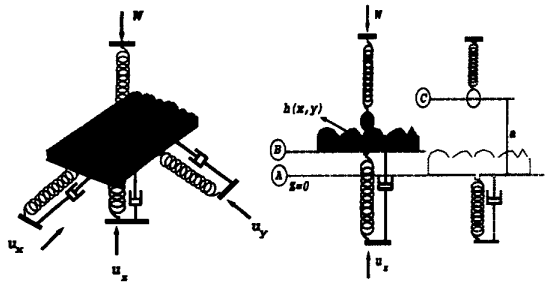

Figure 3: (I) The model for cantilever-sample system. (II) The coordinate systems.

sample, N is the normal force acting between the sample and the cantilever; $F_{r_x} : \mathbb{R} \times \mathbb{R}^6 \to \mathbb{R}$ is given by

$$F_{r_x} = \begin{cases} \left|\frac{F(N)\dot{x}}{\sqrt{\dot{x}^2+\dot{y}^2}}\right| sgn(\dot{x}) & \text{if } \dot{x} \neq 0 \text{ or } \dot{y} \neq 0 \\ F_{a_x} & \text{if } \dot{x} = 0, \dot{y} = 0 \text{ and } \sqrt{F_{a_x}^2 + F_{a_y}^2} \leq |F(N)| \\ \left|\frac{F(N)F_{a_x}}{\sqrt{F_{a_x}^2+F_{a_y}^2}}\right| sgn(F_{a_x}) & \text{otherwise.} \end{cases}$$

F_{r_y} is defined in an analogous manner. Here the friction force $F(N)$ and the force components F_{a_x} and F_{a_y} are given by

$$\begin{aligned} F(N) &= F_{f_s}\left(1+\sqrt{1+\frac{N}{|L_s|}}\right)^{\frac{4}{3}}, \\ F_{a_x} &= m_p u_x(t) - m_p\omega_x^2 x - 2m_p\xi_x\omega_x\dot{x} \\ F_{a_y} &= m_p u_y(t) - m_p\omega_y^2 y - 2m_p\xi_y\omega_y\dot{y}, \end{aligned}$$

where, F_{f_s} and L_s are computed as described in previous section with

$$R_e = R_e(x,y) = \frac{RR_s(x,y)}{R+R_s(x,y)},$$

and R_s equal to the radius of curvature of the sample at the point of contact.

The equation of motion of the cantilever in the inertial frame (represented by C in Figure 3-(II)) is given by $m_c\ddot{q}+m_c\omega_c^2 q = N-W$, where q is the vertical displacement of the cantilever from its mean position and W is the constant forcing. Rewriting these equations in the inertial frame (denoted by A in Figure 3-(II)), by using the relation $z_c = a+q$, where z_c is the z coordinate of the cantilever, we obtain

$$m_c\ddot{z}_c + m_c\omega_c^2(z_c-a) = N-W. \quad (2)$$

The assumption that the sample and the cantilever are always in contact implies that

$$z_c = z + h(x,y) - \delta(x,y) + R, \quad (3)$$

where, $\delta(x,y)$ is the indentation depth and R is the radius of the cantilever tip. By eliminating z and N from equations (1) and (2) and using equation (3), we obtain

$$\begin{aligned} &\ddot{x} + 2\xi_x\omega_x\dot{x} + \omega_x^2 x = u_x(t) - \frac{F_{r_x}}{m_p}, \quad (4) \\ &\ddot{y} + 2\xi_y\omega_y\dot{y} + \omega_y\dot{y} + \omega_y^2 y = u_y(t) - \frac{F_{r_y}}{m_p}, \\ &(1+\frac{1}{\mu})\ddot{z}_c + 2\xi_z\omega_z\dot{z}_c + (\omega_z^2 + \frac{\omega_c^2}{\mu})z_c = u_z(t) + \ddot{h}(x,y) \\ &-\ddot{\delta}(x,y) + 2\xi_z\omega_z(\dot{h}-\dot{\delta}) \\ &+\omega_z^2\left(h(x,y)+R-\delta(x,y)+\frac{\omega_c^2 a}{\mu\omega_z^2}\right) - \frac{W}{m_p}, \\ &N = m_c\ddot{z}_c + m_c\omega_c^2(z_c-a) + W, \end{aligned}$$

where, μ is the mass ratio, $\frac{m_p}{m_c}$ and m_e is the effective mass, $\frac{m_p m_c}{m_p+m_c}$.

2.1 Nondimensionalized Dynamics

In this section, we nondimensionalize the equation (4) by introducing new variables. These variables include x_o, y_o and z_o, the scaling factors in the respective directions; and the scaling frequency ω_o which is used to rescale the time variable. In our simulations (see section 4), x_o and y_o were chosen in the order of atomic diameters; z_o in the order of the cantilever diameter and ω_o in the order of the natural frequency of the cantilever. Using these, we define nondimensional variables as given in Table 1. Note that, by defining a

Old var.	New var.	Relation
x, y, z_c	X, Y, Z	$\frac{x}{x_o}, \frac{y}{y_o}, \frac{z_c}{z_o}$
$t, (\cdot) := \frac{d}{dt}$	$\tau, (\cdot) := \frac{d}{d\tau}$	$\omega_o t, \xi = \frac{d\xi}{d\tau}$
R, A	r, a	$\frac{R}{z_o}, \frac{A}{z_o}$
h, δ	H, Δ	$\frac{h(x,y)}{z_o}, \frac{\delta(x,y)}{z_o}$
$\omega_x, \omega_y, \omega_z, \omega_c$	$\eta_x, \eta_y, \eta_z, \eta_c$	$\frac{\omega_x}{\omega_o}, \frac{\omega_y}{\omega_o}, \frac{\omega_z}{\omega_o}, \frac{\omega_c}{\omega_o}$
u_x, u_y, u_z	U_x, U_y, U_z	$\frac{u_x}{\omega_o^2 x_o}, \frac{u_y}{\omega_o^2 y_o}, \frac{u_z}{\omega_o^2 z_o}$
N, W	N_o, w	$\frac{N}{m_c\omega_o^2 z_o}, \frac{W}{m_c\omega_o^2 z_o}$
F_{r_x}, F_{r_y}	f_{r_x}, f_{r_y}	$\frac{F_{r_x}}{m_p\omega_o^2 x_o}, \frac{F_{r_y}}{m_p\omega_o^2 y_o}$
$\omega_x\ F_{a_x}, F_{a_y}$	f_{a_x}, f_{a_y}	$\frac{F_{a_x}}{m_p\omega_o^2 x_o}, \frac{F_{a_y}}{m_p\omega_o^2 y_o}$

Table 1: Nondimensionalization of the variables.

vector $x = (x_1 \ldots x_6)^T := (X\ \dot{X}\ Y\ \dot{Y}\ Z\ \dot{Z})^T$, we can rewrite equation (4) as

$$\begin{aligned} \dot{x}_1 &= x_2, \quad (5) \\ \dot{x}_2 &= -\eta_x^2 x_1 - 2\xi_x\eta_x x_2 - f_{r_x}(\tau, x) + U_x, \\ \dot{x}_3 &= x_4, \\ \dot{x}_4 &= -\eta_y^2 x_3 - 2\xi_y\eta_y x_4 - f_{r_y}(\tau, x) + U_y, \\ \dot{x}_5 &= x_6, \end{aligned}$$

$$\dot{x}_6 = -\left(\frac{\eta_z^2 + \frac{\eta_c^2}{\mu}}{1+\frac{1}{\mu}}\right)x_5 - \left(\frac{2\xi_z\eta_z}{1+\frac{1}{\mu}}\right)x_6$$
$$+\frac{1}{1+\frac{1}{\mu}}(U_z + \ddot{H} - \ddot{\Delta}) +$$
$$\underbrace{\frac{1}{1+\frac{1}{\mu}}\left(2\xi_z\eta_z(\dot{H}-\dot{\Delta}) + \eta_z^2\left(H + r - \Delta + \frac{\eta_c^2 A}{\mu\eta_z^2}\right) - \frac{w}{\mu}\right)}_{:=\hat{f}_z(\tau)}$$
$$N_o = (\eta_c^2 - \eta_z^2)x_5 - 2\xi_z\eta_z x_6 + \ddot{H} - \ddot{\Delta} + 2\xi_z\eta_z(\dot{H}-\dot{\Delta})$$
$$+\eta_z^2\left(H + r - \Delta - \frac{\eta_c^2 A}{\eta_z^2}\right) + w + U_z.$$

3 Tracking

In this section, we will describe the design of the control laws (U_x, U_y and U_z), so that the piezo moves in a desired manner. We denote the desired trajectories in x, y and z directions by x_r, y_r and z_r (here these trajectories are assumed to be in the nondimensional coordinate system). Normally, in atomic force microscopy, the x_r and y_r are triangular wave signals and z_r is a fixed setpoint. To solve this tracking problem, we convert it into an error stabilization problem. We choose our control signals of the form:

$$U_x(\tau) = -c_x(x_1 - x_r) - c_{\dot{x}}(x_2 - \dot{x}_r) + \ddot{x}_r + \eta_x^2 x_1$$
$$+2\xi_x\eta_x x_2 + v_x,\ U_y(\tau) = -c_y(x_3 - y_r) - c_{\dot{y}}(x_4 - \dot{y}_r)$$
$$+\ddot{y}_r + \eta_y^2 x_3 + 2\xi_y\eta_y x_4 + v_y,\ U_z(\tau) = (\eta_z^2 + \frac{\eta_c^2}{\mu})x_5$$
$$+2\xi_z\eta_z x_6 + (1+\frac{1}{\mu})(-c_z(x_5 - z_r) - c_{\dot{z}}x_6 + v_z) \quad (6)$$

where, $c_{(\cdot)}$ are constants, and $v_{(\cdot)}$ are the control terms to be determined. Now, if we define, $e_x := x_1 - x_r$, $e_y := x_3 - y_r$ and $e_z := x_5 - z_r$, we can write the following time varying *error evolution* equations using equations (5) and (6),

$$\begin{aligned}\ddot{e}_x &= -c_x e_x - c_{\dot{x}}\dot{e}_x + v_x - \hat{f}_x(\tau),\\ \ddot{e}_y &= -c_y e_y - c_{\dot{y}}\dot{e}_y + v_y - \hat{f}_y(\tau),\\ \ddot{e}_z &= -c_z e_z - c_{\dot{z}}\dot{e}_z + v_z + \hat{f}_z(\tau),\end{aligned}$$

where,

$\hat{f}_x(\tau) := f_{r_x}(e_x + x_r, \dot{e}_x + \dot{x}_r, \tau)$ and $\hat{f}_y(\tau) := f_{r_y}(e_y + y_r, \dot{e}_y + \dot{y}_r, \tau)$. This equation, again, can be written as

$$\dot{e} = Ae + B\psi,$$

where,

$$e = (e_x\ \dot{e}_x\ e_y\ \dot{e}_y\ e_z\ \dot{e}_z)^T,$$
$$\psi = (v_x - \hat{f}_x(\tau)\ v_y - \hat{f}_y(\tau)\ v_z - \hat{f}_z(\tau))^T,$$

and

$$A = diag(A_x, A_y, A_z),\ B = diag(B_1, B_2, B_3)$$

with

$$B_i = (0\ \ 1)^T \text{ and } A_{(\cdot)} = \begin{pmatrix} 0 & 1 \\ -c_{(\cdot)} & -c_{\dot{(\cdot)}} \end{pmatrix}.$$

We note that, by choosing the constants, $c_{(\cdot)}$ and $c_{\dot{(\cdot)}}$, we can make the matrix A Hurwitz, and therefore, find symmetric positive definite matrices $P = diag(P_x, P_y, P_z) \in \mathbb{R}^{6\times 6}$ with

$$P_{(\cdot)} = \begin{pmatrix} p_{(\cdot)1} & p_{(\cdot)2} \\ p_{(\cdot)2} & p_{(\cdot)4} \end{pmatrix};\ \text{and } Q \in R^{6\times 6},$$

such that

$$PA + A^T P = -Q.$$

We choose control signals

$$v_{(\cdot)} = -M_{(\cdot)}\ sgn(p_{(\cdot)2}e_{(\cdot)} + p_{(\cdot)4}\dot{e}_{(\cdot)}),$$

where, $M_{(\cdot)}$ are bounds on $|\hat{f}_{(\cdot)}|$. Now, if we consider a Lyapunov function

$$V = e^T P e,$$

we see that
$\dot{V} = -e^T Q e - 2\sum_{i=x,y,z}(p_{i2}e_i + p_{i4}\dot{e}_i)(M_i\ sgn(p_{i2}e_i + p_{i4}\dot{e}_i) - \hat{f}_i(\tau)) < 0$ for $e \neq 0$.

Note that the discontinuities in equation (7) arise due to the terms $\hat{f}(\cdot)$ and existence of the solutions can be shown in the same way as done in [15, 7]. It can also be seen that $M_{(\cdot)}$ are bounds on the corresponding terms in the differential inclusion [15] of this system. Now, we define the function $v : \mathbb{R}\times\mathbb{R}^6 \to \mathbb{R}$ by $v(\tau, e) = V(e)$, and $v_o, v_1 : \mathbb{R}^6 \to \mathbb{R}$ by $v_1(e) = V(e)$ and $v_o(e) = V(e)$; and $w : \mathbb{R}^6 \to \mathbb{R}$ by $w(e) = -e^T Q e$. These functions satisfy all the conditions of Theorem 1 in Section 15 of [7] (pp 153). This shows that the error variables vanish in infinite time. This means that asymptotic tracking is achieved. Another aspect we should be careful of is that all the state variables in equation (5) are bounded as tracking with some state variables growing unbounded is not desirable. Also, since $e_s = s - s_r$ and $\dot{e}_s = \dot{s} - \dot{s}_r$, therefore, $|s| \leq |e_s| + |s_r|$ and $|\dot{s}| \leq |\dot{e}_s| + |\dot{s}_r|$ for $s \in \{x_1, x_3, x_5\}$. This implies that the state variables x_1, x_3 and x_5 and their derivatives are bounded. A good account of this methodology for tracking can be found in [11], pp 190-196.

The control law just described includes a *sgn* function, which is discontinuous and is not desirable as these controllers are hard to implement and may have unwanted effects (for example, chattering). So we replace the *sgn* function by the hyperbolic tangent, $\tanh(\alpha(\cdot))$, $\alpha \in \mathbb{R}$. Note that $\lim_{\alpha\to\infty} tanh(\alpha x) = sgn(x)$. This implies that we can make $|tanh(\alpha x) - sgn(x)|$ arbitrarily small by choosing sufficiently large α for all $x \in \mathbb{R}$. Now, with the hyperbolic tangent function in the control law,

the derivative of the Lyapunov function, $\dot{V} \leq 0$ for all $\|e\| \geq \gamma := \frac{2M_m p_m \rho}{\lambda_{min}(Q)}$, where, $\lambda_{min}(Q)$ is the minimum of the eigenvalues of Q, $M_m = \max_{i \in \{x,y,z\}} M_i$, $p_m = \max_{s \in \mathbb{R}}(|tanh(s) - sgn(s)|$ and $\rho = \max_{s \in \mathbb{R}}(|tanh(s) - sgn(s)|$. This means that this control ensures that the error is inside a ball (of radius γ) in infinite time and this ball can be made arbitrarily small by choosing sufficiently large α. Here too, all the state variables are bounded as in the previous case.

4 Simulation Results

The simulation results of the model described in previous sections are presented in this section. The aim of these simulations is to establish qualitative aspects of the experiments such as 'stick-slip' motion. However, some quantitative inferences can also be made as the values of some physical parameters used in the model have been taken from real experimental data provided in [5]. The shear strength $\tau = 0.91 \times 10^{11}\ Pa$, the reduced elastic modulus, $K = 44.80 \times 10^9\ Pa$, and the interfacial adhesion energy, $\gamma = 0.404\ J/m^2$, are based on [5]. The tip-radius, R, is chosen to be 40 nm, the mass ratio, μ, is assigned a value of 100, the cantilever mass, m_c, is taken to be $6 \times 10^{-9}\ Kg$ and the nondimensional load, w, to be 0.01. The scaling frequency ω_o (which is of the same order as the natural frequency of the cantilever) is equal to $10,000\ rad/sec$, the scaling factors x_o and y_o are given the same value of 2.5 Å (which is of the order of atomic diameters), z_o is set to 100 nm (which is of the order of the cantilever tip diameter). The profile of the test sample was assumed to be $H(x,y) = \beta \sin(k_x x) \sin(k_y y)$, with $\beta = 0.125$ and $k_x = k_y = 0.5$. We assigned $\xi = [0.0366\ 0.0293\ 0.0410]$ and ω (in Hz) = [669.07 407.07 686.13 2400]. These data were obtained from the experiments conducted on the *Digital Instruments Multimode Atomic Force Microscope.*

4.1 Open-loop simulations

In these simulations, the control variables, U_x and U_y in equation (5), were taken only as the reference signals $x_r(\tau)$ and $y_r(\tau)$ respectively. Here, $x_r = y_r := \alpha \sin \omega \tau$ with $\alpha = 20$ and $\omega = 0.005$. Also, it was assumed that the z variable followed a stable dynamics and 'quickly' settled to a predefined setpoint ($z_r = 0.01$). The simulation results of this model are given in the Figures 4 and 6. These figures show that the cantilever 'sticks' to the sample. This is characterized by the horizontal lines in the position-time graph. Also, the graph in Figure 4 matches approximately the graph given in [13], pp 27 (which was obtained experimentally).

4.2 Closed-loop simulations

In these simulations, the same values were used for all the parameters as in the previous simulation, except that the control values U_x and U_y were obtained as described in section 3. The design parameters c_x, $c_{\dot{x}}$, c_y and $c_{\dot{y}}$ are all set to 1.The bounds M_x and M_y are at 15. The matrix P is found by solving the Lyapunov equation with Q being an identity matrix. The simulations described in this section include the z dynamics and control laws as described in section 2. Here, the set point z_r is taken to be 10^{-6}, and the design parameters c_z and $c_{\dot{z}}$ are 2 and 3 respectively. The unknown function $\hat{f}_z(\tau)$ is implemented as a random variable with uniform distribution and bounded by $M_z = 0.05$.

The simulation results of this model are given in Figures 5–6. These figures show that the cantilever does not 'stick' to the sample, but follows the reference signal. The comparison of performance between the open loop and closed loop systems is given in Figure 6. This shows that the controllers achieve good tracking.

Simulations with the hyperbolic tangent function, instead of the signum function, were also performed. In these, the control forces were 'smoother' than when the signum function was used in the control law.

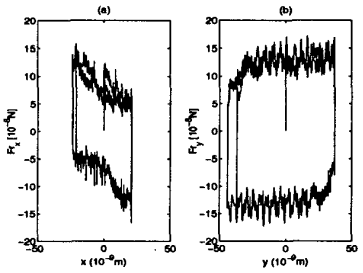

Figure 4: (a) The friction (x-component) vs x graph (b) The friction (y-component) vs y graph.

5 Conclusions

A model for the cantilever-sample dynamics in atomic force microscopy including friction has been developed. The simulations of this model show stick-slip motion, which has been observed in surface force measurements using AFM. A controller was designed to remove 'sticking' and to make the piezo move in a desirable motion. The simulations show that the deviation of the piezo's motion from the desired trajectory is very small.

References

[1] M. Ashhab, M.V. Salapaka, M. Dahleh, and I. Mezić. Dynamical Analysis and Control of Micro Cantilevers. *Automatica*, Accepted, 1998.

[2] B. Bhushan. *Handbook of Micro/Nano Tribology.* CRC Press, 1995.

[3] G. Binnig, C.F. Quate, and Ch. Gerber. Atomic Force Microscope. *Phys. Rev. Lett.*, 56(9):930–933, March 1986.

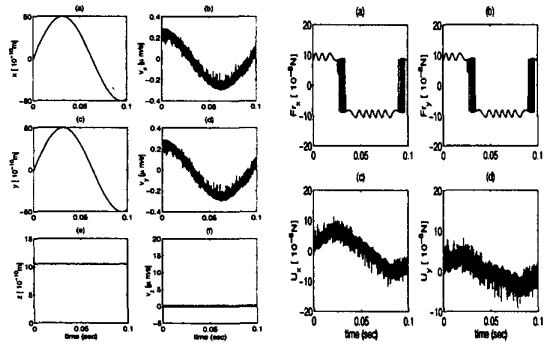

(I) *(II)*

Figure 5: *(I)* (a) and (c): The x and y displacements follow the sinusoidal reference signals. (b) and (d): The corresponding velocities. (e) and (f): z is set to a set point by feedback. *(II)* (a) and (c): The friction and the control forces in x-direction. (b) and (d): Forces in y-direction (closed loop system).

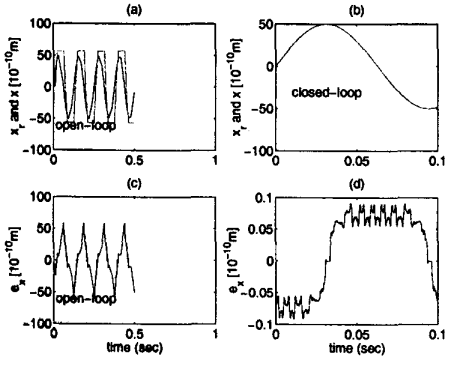

Figure 6: (a): This plot shows the reference or desired signal (the sinusoid) and the displacement x (the jagged line) in open loop configuration. (b): This plot shows the reference and the x signals (the lines appear to have coincided) in the closed loop configuration. (c) and (d): These plots show the difference between the x and the reference signal in the open-loop and closed-loop configurations respectively. Note that the error is greatly reduced in the closed loop.

[4] N.A. et al. Burnham. How Does a Tip Tap? *Nanotechnology*, 8:67–75, 1997.

[5] R.W. Carpick, N. Agrait, D.F. Ogletree, and M. Salmeron. Variation of the Interfacial Shear Strength and Adhesion of a Nanometer-sized Contact. *Langmuir*, 12:3334–3340, 1996.

[6] A. Daniele, S. Salapaka, M.V. Salapaka, and M. Dahleh. Piezoelectric Scanners for Atomic Force Microscopes: Design of Lateral Sensors, Identification and Control. In *Proceedings of the American Control Conference, San Diego*, pages 253–257, June 1999.

[7] A.F. Filippov. *Differential Equations with Discontinuous Righthand Sides.* Kluwer Academic Publishers, 1988.

[8] B.A. Helouvry, P. Dupont, and C. Canudas De Wit. A Survey of Models, Analysis Tools and Compensation Methods for the Control of Machines with Friction. *Automatica*, 30(7):1083–1138, 1994.

[9] A.M. Homola, J.N. Israelachvili, M.L. Gee, and P.M. McGuiggan. *J. Tribol.*, 111:675–, 1989.

[10] J. Hu, X. Xiao, O.F. Ogletree, and M. Salmeron. Atomic Scale Friction and Wear of Mica. *Surface Science*, 327:358–370, 1997.

[11] A. Isidori. *Nonlinear Control Systems.* Springer-Verlag, 2nd edition, 1989.

[12] J. Israelachvili. *Intermolecular & Surface Forces.* Academic Press, 2nd edition, 1991.

[13] B.N.J. Persson. *Sliding Friction.* Springer, 1998.

[14] M.V. Salapaka and D.J. Chen. Stability and Sensitivity Analysis of Periodic Orbits in Tapping Mode Atomic Force Microscopy. In *Proc. of the 37th IEEE Conference on Decision & Control, Tampa, Florida, USA*, pages 2047–2052, December 1998.

[15] S. Salapaka and M. Dahleh. Friction in Atomic Force Microscopy: Modeling and Control. *Technical Report Series, Center for Control Engineering and Computation, UC Santa Barbara*, (CCEC-99-0913), September 1999.

[16] D. Sarid, T.G. Ruskell, R.K. Workman, and D. Chen. Driven Nonlinear Atomic Force Microscopy Cantilevers: From Noncontact to Tapping Modes of Operation. *J. Vac. Sci. Technol. B*, 14(2):864–867, Mar/Apr 1996.

[17] O. Zwörner, H. Hölscher, W. Schwarz, and R. Wisendanger. The Velocity Dependence of Frictional Forces in Point Contact Friction. *Applied Physics A, Materials Science & Processing*, 66:S263–S267, 1998.